Reaction of Phthalate Dioxygenase Reductase with NADH and NAD: Kinetic and Spectral Characterization of Intermediates†

George Gassner, Lihua Wang, Christopher Batie,‡ and David P. Ballou*

Department of Biological Chemistry, University of Michigan, Ann Arbor, Michigan 48109-0606

Received June 8, 1994®

ABSTRACT: Phthalate dioxygenase reductase (PDR) is an electron transferase that contains FMN, which accepts a hydride from NADH, and a [2Fe–2S] center, which transfers electrons to phthalate dioxygenase. The reduction of PDR by NADH has been studied by stopped-flow spectroscopy. Data from studies using both protio- and deuterio-NADH were analyzed by nonlinear curve fitting and numerical simulation techniques. The results of these analyses indicate that the reductive half-reaction of PDR consists of five distinct kinetic phases: (a) NADH binds to form a primary Michaelis complex (MC-1) (K_d = 50 μM). (b) The enzyme undergoes a structural change (116 ± 5 s^{-1}) resulting in a charge-transfer complex (CT-1). (c) The next phase in the reaction shows a deuterium isotope effect of 7.0 when (4*R*)-[^{2}H]NADH (NADD) is substituted for NADH, identifying this step as the one involving hydride transfer. The rate of hydride transfer from NADH to FMN is 70 s^{-1}, and this process results in a charge-transfer intermediate between the flavin hydroquinone anion and NAD (CT*). (d) Internal electron transfer from the flavin to the iron–sulfur center, which is only 35 ± 4 s^{-1}, then results in an intermediate consisting of a reduced [2Fe–2S] center and a neutral flavin semiquinone (SQ). It is surprising that this rate is so slow, since the shortest interatomic distance between these centers is only 4.7 Å [Correll, C. C., *et al.* (1992) *Science 258*, 1604–1610]. The 2-electron-reduced form of PDR (SQ in Figure 1) binds weakly to the reaction product, NAD (K_d = 3.7 mM), but forms a tight complex with NADH (K_d = 10 μM). (e) Two molecules of the reduced iron–sulfur flavin semiquinone (SQ) form of PDR then undergo a relatively slow second-order disproportionation reaction, resulting in one molecule of 3-electron-reduced PDR and one molecule of 1-electron-reduced PDR. The latter reacts rapidly with excess NADH to form a 3-electron-reduced PDR.

Phthalate dioxygenase reductase (PDR[1]) is the iron–sulfur-flavoprotein from *Pseudomonas cepacia* that transfers electrons from NADH to phthalate dioxygenase (Batie *et al.*, 1992, 1987; Batie & Ballou, 1990). The crystal structure of PDR (Correll *et al.*, 1992) reveals three domains, with each monomeric (36 kDa) PDR molecule containing distinct FMN, [2Fe–2S], and NADH binding domains. The FMN and NADH binding domains are highly analogous to the structure of ferredoxin-NADP reductase (FNR) from spinach (Karplus *et al.*, 1991), and the [2Fe–2S] domain of PDR is very similar in structure to plant type ferredoxins (Correll *et al.*, 1992, 1993). Thus, it is thought that PDR can serve as a good model for flavoproteins that transfer electrons between pyridine nucleotides and iron–sulfur centers. Despite this strong structural homology, some experimental evidence (Vieira *et al.*, 1986; Zanetti *et al.*, 1988; Hurley *et al.*, 1993) suggests that the relative orientation of FNR and spinach ferredoxin in the ferredoxin–FNR complex is rotated about 120–180° from that of the [2Fe–2S] and flavin domains of PDR (Correll *et al.*, 1993). This would, nevertheless, preserve the proximity of the [2Fe–2S] and the flavin.

PDR functions by accepting two electrons as a hydride from NADH, and it delivers these as single-electron-reducing equivalents to phthalate dioxygenase (PDO), where they are used for the activation of dioxygen to convert phthalate to *cis*-4,5-dihydrodihydroxyphthalate. In contrast, FNR functions in the reverse manner by accepting low-potential electrons from spinach ferredoxin and transferring a hydride to NADP. The redox potentials for these systems are appropriate for their corresponding directions of electron flow. In the case of PDR, the calculated midpoint potential for the flavin-oxidized/2-electron-reduced couple (–231 mV) is 80 mV more positive than that for the NADH/NAD couple (–311 mV at 25 C, pH 7) (Clark, 1960). The flavin semiquinone/fully reduced redox couple (–287 mV at pH 7 and 25 °C) is 113 mV more negative than the [2Fe–2S] and flavin oxidized/semiquinone potentials (both are about –174 mV at pH 7 and 25 °C). In contrast, the single-electron-reduction potential for ferredoxin is –505 mV in the FNR–ferredoxin complex at pH 9, which is 60 mV more negative than the midpoint potential for the 2-electron reduction of FNR (–445 mV) (Batie *et al.*, 1981). The midpoint potential of the NADP/NADPH couple at pH 9 and 30 °C is –377 mV (Clark, 1960). This is 68 mV more positive than that for the FNR flavin oxidized/2-electron-reduced couple. Thus, while the structural organization of PDR and ferredoxin-NADP reductase is clearly related in these electron transferases, nuances in the environment brought about by the properties of the individual proteins modify the potentials of the redox centers for carrying out their respective functions (Correll *et al.*, 1993).

The transformation of pyridine nucleotide hydride equivalents to single-electron-reducing equivalents, followed by electron transfer to iron–sulfur center acceptors, is a recurrent theme in the biochemical pathways of respiration and photosynthesis (Kamin *et al.*, 1980), as well as in the electron transport pathways for various cytochrome P-450-containing

† Supported by a grant from the U.S. Public Health Service (GM 20877 to D.P.B.).

* Author to whom correspondence should be addressed.

‡ Present address: Department of Biochemistry, Louisiana State University Medical Center, New Orleans, LA 70112.

® Abstract published in *Advance ACS Abstracts,* September 15, 1994.

[1] Abbreviations: PDR, phthalate dioxygenase reductase; FNR, ferredoxin NADP reductase; $FMNH^-$, reduced FMN anion; $FMNH^•$, neutral blue FMN semiquinone; [2Fe–2S], two iron, two sulfur redox center; NHE, normal hydrogen electrode; NADD, reduced nicotinamide adenine dinucleotide deuterated in the 4*R* position.

0006-2960/94/0433-12184$04.50/0

and other oxygenase and desaturase systems. The mechanism and intermediates involved in the reductive half-reaction of PDR probably are also representative of those occurring in the analogous electron-transfer components of other bacterial dioxygenases involved in biodegradation (Batie *et al.*, 1992), especially those like the closely related naphthalene oxygenase reductase (Mason & Cammack, 1992). The reductive half-reaction of PDR may also share common features with the monomeric, iron–sulfur flavoprotein reductase component of methane monooxygenase (Lund *et al.*, 1985). Therefore, an understanding of the reductive half-reaction of PDR may be of broad significance.

We report here a detailed study of the kinetics and mechanism of the reductive half-reaction of PDR with NADH, which can serve as a model for several other electron transport systems. The proposed mechanism (Scheme 1) can quantitatively account for all of our data. The spectra of the intermediate species derived from simulation of the data by this mechanism are consistent with those expected for the chemical species proposed in the mechanism.

MATERIALS AND METHODS

PDR was isolated from *Pseudomonas cepacia* DB01 and purified as previously reported (Batie *et al.*, 1987). (4*R*)-[2H]NADH was synthesized following a procedure similar to that described by Loesche *et al.* (1980). Yeast alcohol dehydrogenase (0.2 mg) and NAD (25 mg) were combined in 5 mL of 0.1 M NH_4HCO_3 buffer (pH 7.0) containing 0.3 mL of CD_3CD_2OH. The formation of (4*R*)-[^{2}H]NADH (NADD) was monitored at 340 nm, and the reaction was complete within 15 min. Alcohol dehydrogenase was removed immediately after completion of the reaction by ultrafiltration over Centricon-30 microconcentrators. The filtrate was diluted 5-fold in glass-distilled H_2O and applied to a 5 × 1.5 cm Fast Flow DEAE Sepharose (Pharmacia) column (HCO_3^- form). NADD eluted about midway through a 300 mL gradient (0–0.2 M NH_4HCO_3). Pooled fractions containing NADD were found to have $A_{260}/A_{340} = 2.6$. NH_4HCO_3 was removed by 3–4 cycles of rotary evaporation, which were followed by resuspension in H_2O. NADH was produced by the same procedure, but using nondeuterated ethanol. The kinetics of reduction of PDR with NADH either purchased from Boehringer Mannheim or produced by the above synthesis was indistinguishable.

Kinetic data were acquired using either a Kinetic Instruments, Inc., stopped-flow spectrophotometer using program A with a DOS-based computer or a Hi-Tech Scientific Model SF-61 stopped-flow spectrophotometer that was controlled by a Macintosh IIcx using KISS software (Kinetic Instruments, Inc.). The Kinetic Instruments stopped-flow spectrophotometer was equipped with a custom mixer for dissimilar solvents and consequently exhibited a longer than normal dead time. Dead times were determined to be 3.8 ms for the Kinetic Instruments system and 2 ms for the Hi-Tech system. Both instruments were used in the single-wavelength mode with photomultiplier detection. The Hi-Tech instrument was set up for rapid scanning (quick scan feature), allowing for collection of high-quality spectra at 200 nm/s. The Kinetic Instruments stopped-flow instrument was equipped with a Princeton Instruments ST1000 diode array detector in addition to the photomultiplier detector. When operated in the diode array detection mode, it could record spectra every 4 ms during the reaction.

All kinetic experiments were performed at 4 °C in anaerobic, filtered 100 mM HEPES, pH 8.0, containing *ca.* 1 μM protocatechuate dioxygenase (PCD) and 100 μM protocatechuate (PCA) as an oxygen-scavenging system (Bull & Ballou, 1981). Samples containing PCD were vacuum gas exchanged in tonometers and overlaid with *ca.* 2 psi of argon containing ≤0.5 ppm of O_2. After several rounds of gas exchange, protocatechuate was added from a side arm of the tonometer.

Two primary methods have been employed for the analysis of kinetic data from these experiments: data fitting to analytical expressions and data simulation. Using a consecutive exponential fitting routine based on the Marquardt–Levenberg algorithm (Bevington, 1969), the data were fit with up to five irreversible exponential steps. Since the model (Scheme 1) cannot be fit to an analytical expression, the experimental data were then simulated using a fourth-order Runge–Kutta numerical algorithm (Press *et al.*, 1992). The Marquardt–Levenberg routines were useful in obtaining estimates of rate constants and amplitudes for the multiple phases of the reaction. These estimates could then be refined and adapted to simulations that used the Runge–Kutta algorithm. The simulations were carried out for data recorded at certain wavelengths using a wide range of NADH concentrations. The kinetic parameters used for the simulations were varied until a single set of rate constants could fit all of this data. Simulations of the concentration profiles thus determined were then fit with a least-squares routine to data that had been recorded at wavelength increments across the visible range to determine the spectra of intermediates. Both the simulation and the fitting routines are built-in features of program A for PC-compatible computers; this program for analyzing and collecting data was written in this laboratory by Joel Dinverno, Chung-Jen Chiu, and Rong Chang. Some of the simulations were carried out using the KSIM program from Hi-Tech, Ltd., and the HopKINSIM program for Macintosh, adapted by Danny Wachstock (1990 version) from the KINSIM program by Barshop *et al.* (1983) and Zimmerle and Frieden (1989).

RESULTS

Spectroscopic and Redox Properties. Oxidized PDR is an orange-brown protein with the absorbance spectrum shown in Figure 1C. This spectrum is consistent with the sum of the spectra of bound, oxidized flavin (FMN), which absorbs in the 300–500 nm region (shown for the FAD in FNR in Figure 1A), and a [2Fe–2S] center, which absorbs between 300 and 800 nm (shown for adrenodoxin Figure 1B) (Batie *et al.*, 1987).

The redox potentials of PDR have been determined by anaerobic titration with dithionite, utilizing the redox dyes anthraquinone-2,6-disulfonate (–184 mV) or safranine-O (–289 mV), to monitor the potential. At pH 7.0, the potentials of the [2Fe–2S] couple and the $FMNH^{\bullet}/FMN$ couple are essentially identical (–0.174 V vs NHE). The potential of the $FMNH^-/FMNH^{\bullet}$ couple is –0.287 V (vs NHE). Thus, during titration of PDR with dithionite, the first two electrons simultaneously produce a reduced [2Fe–2S] center and the semiquinone form of the flavin. Consistent with this, the spectrum of the 2-electron-reduced PDR (Figure 1C) is similar to the sum of the FNR semiquinone spectrum (Figure 1A) and the reduced adrenodoxin spectrum (Figure 1B). The third electron, which produces fully reduced enzyme, titrates in at a lower potential. The spectrum of 3-electron-reduced PDR (Figure 1C) is also similar to the sum of the spectra from fully reduced FNR (Figure 1A) and reduced adrenodoxin (Figure 1B).

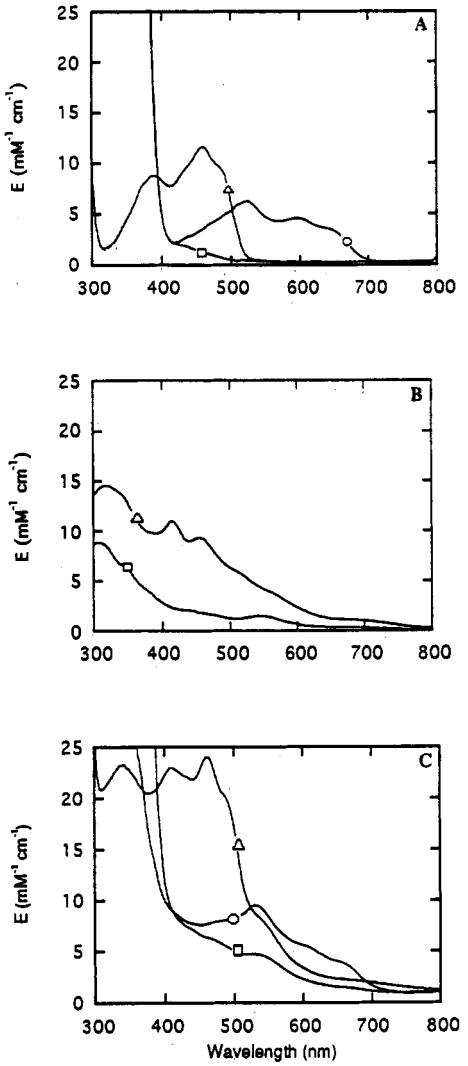

FIGURE 1: Spectra of (A) FNR (△) oxidized, (○) semiquinone, (□) and reduced; (B) adrenodoxin (△) oxidized and (□) reduced; (C) PDR (△) oxidized, (○) 2-electron-reduced, and (□) 3-electron-reduced.

Overview of the Kinetics of the Reductive Half-Reaction. The reduction of PDR by NADH is via hydride transfer, mandating that it occurs in discrete 2-electron steps. Figure 2 shows the overall process of reduction of PDR (on two different time scales) by excess NADH. Part A shows selected spectra from the first 120 ms of the reaction. The data were recorded on the Kinetic Instruments stopped-flow instrument using a diode array detector (4 ms/spectrum). By 120 ms after mixing, a neutral blue semiquinone and a reduced [2Fe–2S] center are formed, indicating that the first 2-electron reduction is complete at this time. The spectra shown in part B were recorded with the quick scan feature of the Hi-Tech/KISS stopped-flow spectrophotometer (3 s/spectrum). During this period, the 2-electron-reduced PDR undergoes a slow second-order disproportionation reaction and is further reduced by excess NADH to fully reduced PDR.

Preliminary studies of the reductive half-reaction of PDR (Batie & Ballou, 1987) indicated that the reaction was characterized by four distinct kinetic phases (three phases before 120 ms and one phase afterward). These phases are observable at wavelengths across the visible spectrum. In this paper, we have used the dependence on NADH concentration and deuterium isotope effects in combination with the interpretation of calculated absorbance spectra to assign the redox states of the observed reaction intermediates. Kinetic

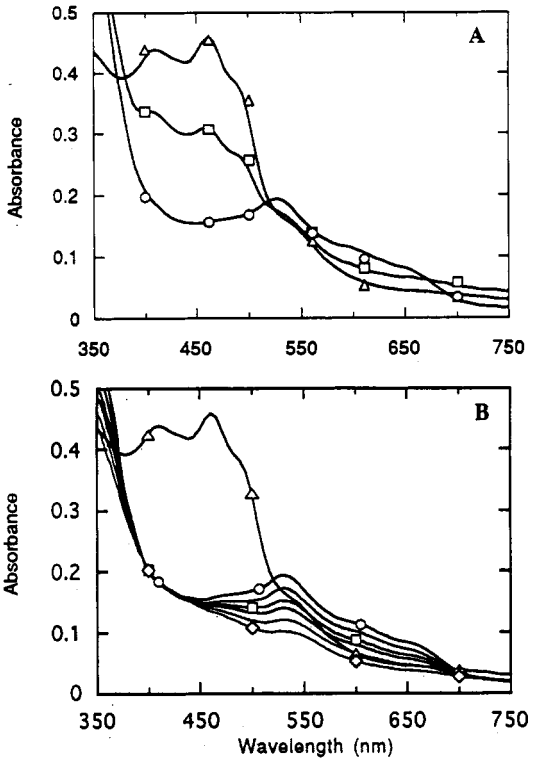

FIGURE 2: Spectra of PDR reacting with excess NADH: (A) 4 ms diode array recordings of spectra occurring during the first 120 ms of the reaction between 20 μM PDR and 100 μM NADH. Average time of the recording after mixing: (△) 2 ms (note that the solid line is the spectrum of oxidized PDR, *i.e.*, the starting spectrum before the addition of NADH, and is identical to the starting spectrum in part B); (□) 34 ms; (○) 118 ms. The symbols identifying the spectra are also points calculated from simulations of the data at the times of the spectra. See text for explanations. (B) 3 s quick scan spectra recorded during the reaction of 20 μM PDR with 50 μM NADH. Average time of the recording after mixing: (△) starting spectrum before addition of NADH; (○) 1.5 s; (no symbol) 13 s; (□) 34 s; (no symbol) 56 s; (no symbol) 2 min; (◇) 7 min.

traces at 462, 610, and 740 nm were used to study the NADH and NAD concentration dependencies and the deuterium isotope effects (Figures 3 and 4). Absorbance changes at 462 nm were monitored, where both the FMN and the [2Fe–2S] center absorb strongly (Figures 2–4). Data collected at 610 nm provide the clearest information on the formation and decay of the flavin semiquinone (Figures 1, 3, and 4). Charge-transfer complexes between the flavin and nicotinamide (Massey & Palmer, 1962; Lambeth & Kamin, 1976, 1979; Massey & Ghisla, 1974; Zipples & Staab, 1984; Shieh *et al.*, 1981; Shoun *et al.*, 1979; Howell *et al.*, 1972) were detected at 740 nm (Figures 3 and 4).

Concentration Dependence of the Reaction of PDR with NADH. There are five steps in the reductive half-reaction of PDR (Scheme 1, Figure 3) occurring within the first second after mixing with NADH. At one second after mixing PDR and excess NADH, one observes a composite spectrum of a reduced iron–sulfur center and a flavin semiquinone (MC-3 in Scheme 1, Figure 2B). The first step shows no significant absorbance changes, but is inferred from the kinetic behavior (see below). In the second step the absorbance between 400 and 500 nm decreases slightly and a weak long wavelength absorbance develops, consistent with a charge-transfer interaction between NADH and oxidized flavin (Scheme 1, CT-1) as observed for other flavoproteins (Massey & Ghisla, 1974). This process occurs largely in the first 10 ms of the reaction and is indicated in Figure 3 by the vertical bar labeled I. The kinetic dependence on NADH concentration of the

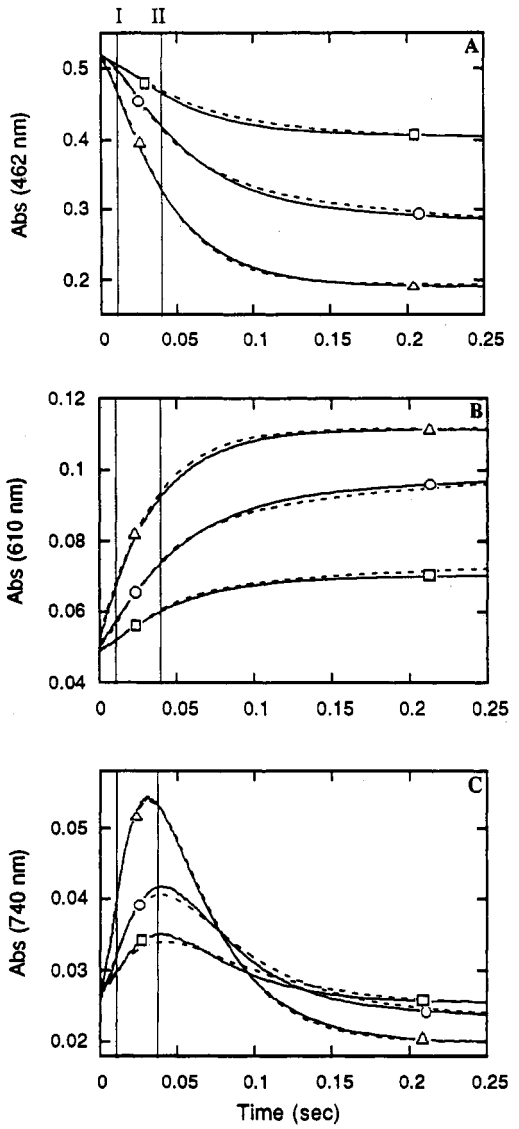

FIGURE 3: Reaction traces (—) of PDR (20 μM) reacting with various concentrations of NADH [(△) 100 μM, (○) 20 μM, (□) 10 μM] at (A) 462, (B) 610, and (C) 740 nm, and simulations (---) according to Scheme 1.

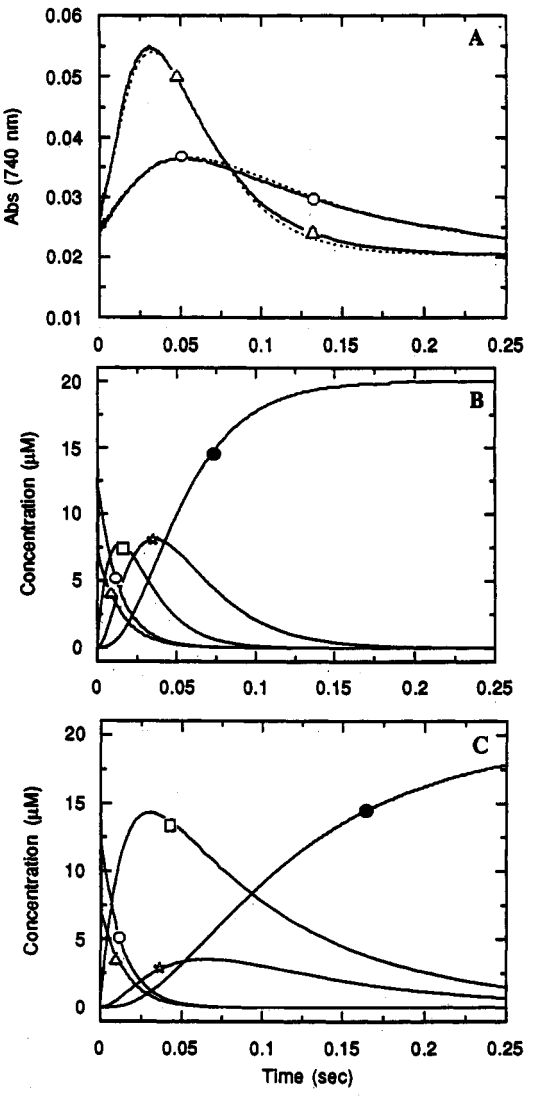

FIGURE 4: (A) Reaction traces recorded at 740 nm for reactions with PDR (20 μM) using (△) 250 μM NADH or (○) 250 μM NADD: data (—) and simulations (---). Simulations were according to Scheme 1 using the extinction coefficients of Table 1. (B) Simulations showing the concentrations of the various species occurring during the reaction as in A for NADH. (C) Simulations showing the concentrations of the various species occurring during the reaction as in A for NADD: (○) PDR_{ox}; (△) MC-1; (□) CT-1; (☆) CT*; (●) SQ + MC-3.

formation of CT-1 indicates saturation behavior (Strickland *et al.*, 1975) requiring the inclusion of the first rapid equilibrium step to form MC-1, as shown in Scheme 1. Comparison of simulations to data collected under second-order reaction conditions led to an estimated K_d of 50 μM for MC-1 formation. The third step shows significant increases in absorbance at wavelengths greater than 500 nm and decreases in absorbance below 500 nm. This process occurs principally between labels I and II of Figure 3 and is due to the reduction of the flavin and formation of a charge-transfer complex (described as CT*) between the flavin hydroquinone anion and the NAD. This assignment comes from studies employing isotopically labeled NADD and will be described in the next section. In the fourth step (between labels II and about 0.15 s in Figure 3), NAD is released (at 35 s^{-1}) and one electron is transferred from the reduced flavin to the [2Fe–2S] center. On the basis of kinetic data, NAD release and electron transfer occur at the same rate; however, we cannot distinguish whether this is a sequential or a concerted event. Release leads to the loss of the charge-transfer absorbance at long wavelengths and to an increase in absorbance at 610 nm due to the formation of flavin semiquinone. In the fifth step NADH rebinds to the 2-electron-reduced PDR to produce MC-3, accompanied by small further decreases in long wavelength absorbance. MC-3 is observed only when excess NADH is used. From studies of the dependence of the fifth step on NADH concentration, a K_d of 10 μM could be estimated. Details of the kinetic rationale for these assignments are described in the following sections.

Deuterium Isotope Effect. To define the step involving hydride transfer from NADH to FMN, experiments were carried out using NADH and (4*R*)-[^{2}H]NADH. Data collected at 740, 610, and 462 nm were simulated in accordance with the model outlined in Scheme 1 using both NADH and (4*R*)-[^{2}H]NADH, each at several concentrations. Data recorded at 740 nm and simulations are shown in Figure 4. These simulations require a 7-fold deuterium isotope effect on the third step of the reduction (Scheme 1) in which CT* forms. Intramolecular electron transfer from the reduced flavin anion to the iron–sulfur center, identified with step 4, occurs at 35 ± 4 s^{-1} and is not affected by the deuterium substitution. Thus, upon substitution of (4*R*)-[^{2}H]NADH for NADH, deuteride transfer (10 s^{-1}) from the NADD to

Scheme 1: Proposed Mechanism of the Reductive Half-Reaction for PDR[a]

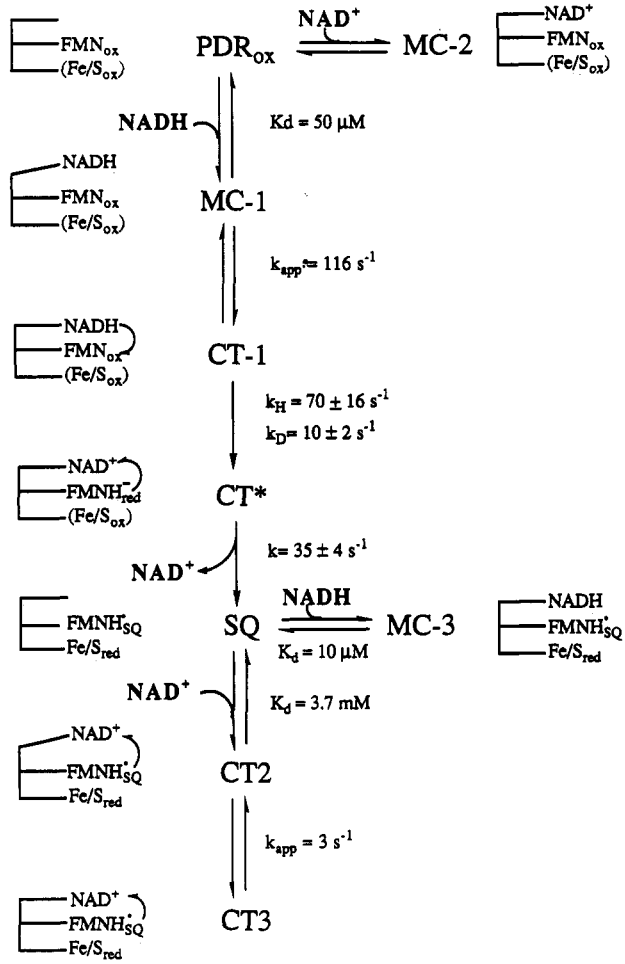

[a] The values for the rate constants were determined from fitting procedures and simulations as described in the text.

the FMN (a process that forms CT*) is slower than intramolecular electron transfer (which converts CT* to SQ), whereas in the presence of NADH, hydride transfer is faster (70 s^{-1}) than electron transfer. Therefore, with NADD as substrate a smaller amount of CT* is observed than in the presence of NADH. This is illustrated in Figure 4B,C, in which the concentrations of the various intermediates are plotted as a function of time for reactions using both NADH and NADD. As expected, in the presence of NADD an increased amount of CT-1 forms.

Fitting the data recorded at 740 (Figure 4) and 462 nm (data not shown) with an unrestricted Marquardt–Levenberg nonlinear least-squares fitting routine to a simple sequential model would indicate that there is a deuterium isotope effect of only about 3-fold on the decay of CT*. However, if the isotope effect were actually on this decay step, one would expect to accumulate more of the CT* intermediate when using NADD than when using NADH. This clearly is not the case, as is shown in Figure 4. Thus, the isotope effect is actually on the formation of CT*. Since the rate constants for formation and decay of CT* are similar in magnitude, any isotope effect on the formation rate constant will kinetically have an apparently coupled effect on the observed decay rate constant. Although standard computer fitting to two sequential exponential reactions does give excellent fits, indicating a 3-fold deuterium isotope effect, such results would also require the extinction coefficient for the charge-transfer intermediate CT* to decrease by about 40% with deuterium substitution, a rather unsatisfactory conclusion. Thus, the key to understanding the deuterium isotope effect comes from the amplitude data.

It was proposed earlier that the step involving the decay of absorbance at 740 nm corresponded to the hydride transfer from NADH to PDR and that intramolecular electron transfer from the flavin to the iron–sulfur center was very fast and not directly observable (Batie & Ballou, 1987). The proximity of the flavin and iron–sulfur clusters in the crystal structure favored this hypothesis (Correll *et al.*, 1992). The preceding results now contradict this proposal (see Discussion). In addition, these results clearly show that PDR uses the A-side hydrogen (*pro-R*) from NADH (You, 1982).

Complexes of NADH and NAD with the Reduced Iron–Sulfur Flavin Semiquinone Form of PDR. Although simulation of the model (Scheme 1), including steps up to the formation of SQ, could account for the deuterium isotope effect at multiple wavelengths, it failed to describe the NADH concentration dependence of the reaction following intramolecular electron transfer (notice the relative absorbance of the shots at 740 nm between 150 and 250 ms in Figure 3C). We postulated that as the reduced iron–sulfur semiquinone intermediate, SQ, releases NAD, the NADH in solution rapidly binds to the enzyme, decreasing the long wavelength absorbance of the 2-electron-reduced PDR, as shown in Scheme 1 (step showing the formation of MC-3). By incorporating this quite logical step into the model, it was possible to simulate the data over the entire concentration range at all wavelengths using chemically reasonable extinction coefficients and a single set of rate constants. These simulations indicate that the K_d of the SQ–NADH complex (which is called MC-3) is about 10 μM.

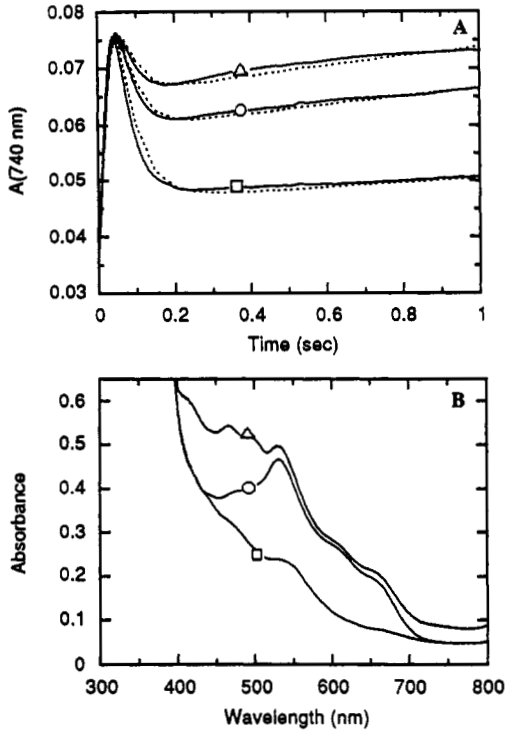

FIGURE 5: (A) Traces recorded at 740 nm for 20 μM PDR reacting with 17.4 μM NADH in the presence of various concentrations of excess NAD: (△) 8 mM NAD; (○) 4 mM NAD; (□) 1 mM NAD; (—) data; (---) simulations. (B) Spectra recorded using the quick scan feature (see Materials and Methods) during reactions that included 20 μM PDR and (△) 17.4 μM NADH and 4 mM NAD, with scan between 0.5 and 3 s; (○) 100 μM NADH and no NAD, with scan between 0.5 and 3 s; (□) 100 μM NADH and no NAD, spectrum recorded after 10 min.

In the presence of excess NAD, two additional charge-transfer complexes follow the formation of CT* (CT-2 and CT-3 in Scheme 1). The charge-transfer complex (CT-2) between NAD and the SQ form of PDR was generated by anaerobically mixing oxidized PDR with stoichiometric NADH and excess NAD. CT-2 is distinguished from CT* by two criteria: (a) CT-2 forms only after NAD is released from CT*, as is apparent in the decrease in CT* absorbance at 740 nm prior to CT-2 formation (Figure 5A), and (b) the spectral properties of CT-2 (Figure 5B) are significantly different than those of CT* (as shown in Figure 6). In Figure 5B, spectra are shown indicating the properties of CT-1 and MC-3 pointing out these features. The top spectrum is composed primarily of a mixture of oxidized PDR (PDR_{ox}), CT-2, and CT-3. The absorbance beyond 700 nm attributed to CT-2 and CT-3 is the most notable feature. In addition to the long wavelength charge-transfer band, CT-2 has spectral features similar to those of the semiquinone rather than to those of the reduced form of the enzyme (Figures 2 and 5B). For comparison, Figure 5B shows a spectrum primarily of MC-3, which is the NADH complex of SQ. Analysis of the dependence of the formation of CT-2 on the NAD concentration permitted the determination of a $K_d \sim 3.7$ mM for binding NAD to SQ. Within 1 s after mixing (after which 2-electron-reduced PDR begins to disproportionate), CT-2 apparently isomerizes to form yet another charge-transfer complex, CT-3 (Figure 5A). CT-3 has more intense absorbance at long wavelengths (>700 nm) than CT-2. The data suggest that the transition from CT-2 to CT-3 involves a slow conformational change and that the formation of both of CT-2 and CT-3 depends on the NAD concentration. Data obtained at various NAD concentrations can be simulated by including

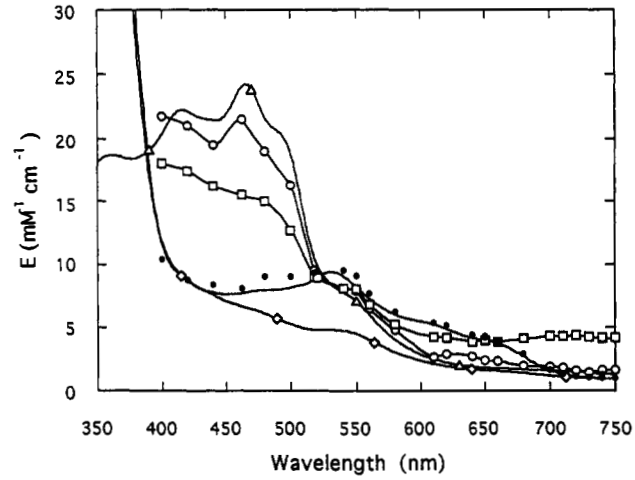

FIGURE 6: Spectra of the intermediates involved in the reduction of PDR. Spectra were derived from simulations according to Scheme 1 of the data recorded at each wavelength shown. Details are in the text: (△) PDR_{ox} (the solid line is the same as the starting spectrum in Figure 2); (○) CT-1; (□) CT*; (●) MC-3 (the solid line is the same as the spectrum recorded at 1.5 s in Figure 2B); (◇) PDR_{3e^-} (the solid line is the same as the spectrum recorded at 7 min in Figure 2B).

the NAD binding steps in the bottom of the model as shown in Scheme 1. This model proposes that CT-2 and CT-3 are interconverted through a slow, reversible isomerization and that both species are in rapid equilibrium with NAD. Simulation of CT-2 and CT-3 formation supports K_d values of 3.7 mM for both complexes and predicts an apparent isomerization rate of ~ 3 s^{-1}. Other equivalent models can also fit the data, and at this point we cannot distinguish such models from the current general model. When very high concentrations of NAD were included in these experiments, a lag became apparent in the first observed kinetic phase, which is consistent with competition between NAD and NADH for binding to the oxidized enzyme. These data suggest that NAD binds with low affinity ($K_d > 1$ mM). We designate the oxidized PDR/NAD complex as MC-2 (Scheme 1).

Disproportionation of the Reduced Iron–Sulfur Flavin Semiquinone Form of PDR. The slow last phase of the reaction of PDR with NADH involves a second-order, bimolecular disproportionation of electrons between MC-3 molecules. Figure 2B shows the spectral changes occurring during this reaction. A proposed mechanism for this disproportionation reaction is shown in Scheme 2. First, NADH binds to the 2-electron-reduced SQ form of PDR in a rapid equilibrium step to form the NADH·PDR_{2e^-} complex (also called MC-3). Then, two MC-3 molecules undergo a rate-limiting disproportionation reaction to form one fully reduced PDR_{3e^-} and one NADH·PDR_{1e^-} complex; the latter is rapidly reduced to PDR_{3e^-} by the associated NADH. Simulations of the NADH concentration dependence of this reaction according to the model of Scheme 2 permitted an estimation of the K_d for MC-3 formation of 16 ± 5 μM. This is similar to the value (10 μM) obtained from the simulations of reduction kinetics through the formation of MC-3 (Scheme 1). The calculated second-order rate constant of the disproportionation reaction of NADH·PDR_{2e^-} is 800 ± 100 M^{-1} s^{-1}.

Spectra of Intermediates. Kinetic traces recorded at intervals of 10–20 nm between 420 and 750 nm during the reduction of oxidized enzyme by saturating NADH were simulated by using the proposed model of Scheme 1. By applying absorbance coefficients that best fit the data at each wavelength, it was possible to generate spectra for each

Scheme 2: Proposed Mechanism for the Disproportionation of MC-3 and the Formation of 3-Electron-Reduced PDR

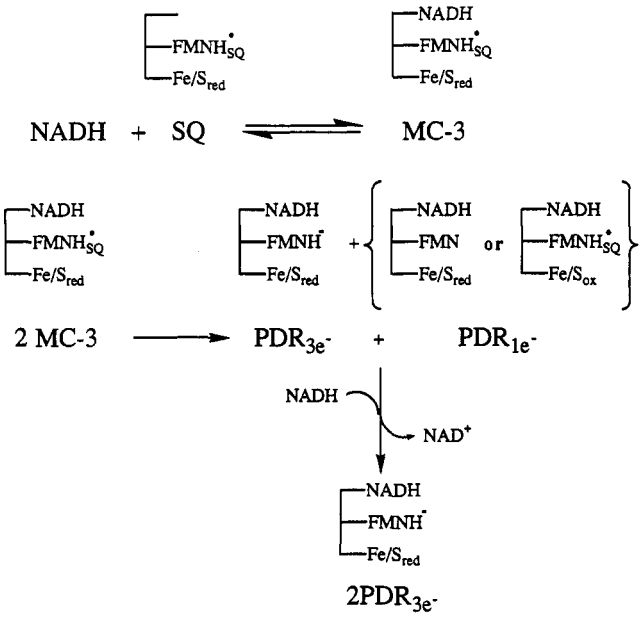

intermediate (Figure 6). The CT* spectrum generated from these simulations resembles the spectrum of oxidized [2Fe–2S] and reduced flavin plus a long wavelength $FMNH^- \rightarrow$ NAD charge-transfer band (Howell & Massey, 1972; Shoun *et al.*, 1979; Lambeth & Kamin, 1976). These simulated spectra, and the data collected by diode array rapid scanning (see below), have identified the intermediate penultimate to the disproportionation reaction (MC-3 in Figure 2B) as a form containing both $[2Fe–2S]_{red}$ and the neutral blue flavin semiquinone.

The reductive half-reaction of PDR has also been studied by stopped-flow spectroscopy with diode array detection. In these experiments, spectra can be recorded every 4 ms during the reaction. Figure 2A shows spectra taken at 2, 34, and 118 ms during the reaction of 20 μM PDR with 100 μM NADH. By simulating the reaction according to the proposed scheme and employing the extinction coefficients of the intermediate species at appropriate wavelengths (Table 1), we can generate spectra for any time point during the reaction. Figure 2 shows excellent agreement of the calculated spectral points with the spectra obtained by diode array stopped-flow spectroscopy. This further supports the assignment of intermediates and rate constants. The extinction values we report for the CT* complex are significantly larger than those reported for related systems (Figure 6 and Table I).

DISCUSSION

Spectra of Intermediates. We have deduced a mechanism for the reduction of PDR by NADH (Scheme 1) that accounts for the observed kinetics at all wavelengths examined. Moreover, the spectra derived from the kinetic analysis for intermediates are equivalent to the sum of the spectra of iron–sulfur and flavin centers in the appropriate redox states previously observed in other related enzymes (Figure 1 and Table 1). The spectra of the intermediates (Figure 6) were obtained by simulating the kinetic traces across the visible wavelength range using the mechanism in Scheme 1. The initial Michaelis complex (MC-1) has essentially the same spectrum as oxidized PDR. CT-1 has spectral properties similar to those of the NADPH $\rightarrow$ FAD (oxidized) charge-transfer complex of FNR (Batie *et al.*, 1986) superimposed on an oxidized [2Fe–2S] ferredoxin type spectrum, such as adrenodoxin (Kimura & Suzuki, 1967), spinach ferredoxin (Palmer & Fee, 1971), putidaredoxin (Cushman *et al.*, 1967), or xanthine dehydrogenase (Nishino *et al.*, 1989) (Figure 1B). The calculated spectrum of CT* is consistent with the sum of the spectrum of an oxidized [2Fe–2S] ferredoxin center (Figure 1B) plus the spectrum of a charge-transfer complex of reduced flavin anion to oxidized pyridine nucleotide, such as those observed in *p*-hydroxybenzoate hydroxylase (Howell & Massey, 1972; Shoun *et al.*, 1979) and adrenodoxin reductase (Lambeth & Kamin, 1976). Our calculated spectrum of MC-3, the reduced iron–sulfur/flavin semiquinone form of PDR in a complex with NADH, has extinctions that closely match the sum of the spectrum of the neutral blue semiquinone observed in FNR (Figure 1), flavodoxin (Mayhew, 1970), or cytochrome P-450 reductase (Iyanagi *et al.*, 1974) plus the spectrum of reduced ferredoxin (Nishino *et al.*, 1989; Palmer & Fee, 1971; Kimura & Suzuki, 1967; Cushman *et al.*, 1967) (see Table 1 for a partial listing). Finally, the charge-transfer intermediates, CT-2 and CT-3, have long wavelength spectral features consistent with both flavin $\rightarrow$ pyridine nucleotide charge-transfer interactions and visible features characteristic of a blue flavin semiquinone. Time-resolved spectra generated by simulating the mechanism in Scheme 1 (see Figure 2, which shows points fitted for selected wavelengths) are in excellent agreement with diode array data recorded during the reaction. We have thus outlined a chemically logical mechanism that is internally consistent with all of our kinetic data.

Binding of NADH to PDR. In agreement with earlier work (Batie & Ballou, 1987), we found it necessary to include a two-step binding reaction with NADH that involves both a Michaelis complex, MC-1, and a charge-transfer complex between NADH and FMN, identified as CT-1. Conversion between these two forms may represent a conformational change in the protein as implied in Scheme 1. The crystal structure of oxidized PDR solved by Correll *et al.* (1992) reveals that a phenylalanine (Phe225) stacks with the isoalloxazine ring of the flavin. It was suggested that the phenylalanine ring in PDR forms a gate separating the flavin from the NADH binding site (Correll *et al.*, 1992), such that this phenylalanine ring must swing out of the way to allow the nicotinamide ring of NADH to approach the flavin for hydride transfer. This is fully consistent with the two-step binding mechanism predicted from our kinetic analysis, such that MC-1 may represent the complex of NADH with oxidized PDR before Phe225 moves away. The second binding intermediate, CT-1, could represent the state of the enzyme after it has undergone a structural change to open the phenylalanine gate, thereby permitting the nicotinamide ring to interact with the oxidized flavin in preparation for hydride transfer. The spectrum of CT-1 is consistent with it being an NADH $\rightarrow$ flavin charge-transfer complex (Figure 6) (Howell *et al.*, 1972; Batie & Kamin 1986). Similarly, in FNR, Tyr314 resides between the nicotinamide ring of NADPH and the isoalloxazine ring of FAD (Karplus *et al.*, 1991). This tyrosine presumably swings out of the way to allow direct interaction followed by hydride transfer from NADPH to FAD. In glutathione reductase, Tyr197 presumably serves an analogous role (Pai *et al.*, 1988; Karplus & Schultz, 1989). However, the charge-transfer interaction in glutathione reductase is more complex: both the Cys63 thiol and NADPH interact with FAD.

Deuterium Isotope Effects. The results of deuterium isotope effect studies led us to assign the second spectrally observed

Table 1: Comparison of Spectral Properties of PDR with Those of Related Systems

intermediate species	ext (M^{-1} cm^{-1}) at 462 nm (A)	ext (M^{-1} cm^{-1}) at 610 nm (B)	ext (M^{-1} cm^{-1}) at 740 nm (C)	extinctions of flavin and pyridine nucleotide charge–transfer complexes (D)	oxidized and reduced ferredoxin extinctions (E)	sums of extinctions from related systems (D + E)
PDR (ox)	24000	2470	1310	FNR (ox)[a] 10300 M^{-1} cm^{-1} (462 nm)	[2Fe–2S] (ox)[d] 9200 M^{-1} cm^{-1} (462 nm)	19500 M^{-1} cm^{-1} (462 nm)
MC-1	23330 ± 1200	2400 ± 130	1280 ± 100			
CT-1	21480 ± 700	3440 ± 620	1960 ± 570	{NADH → FNR (ox)}[a] 1400 M^{-1} cm^{-1} (610 nm)	[2Fe–2S] (ox)[d] 2000 M^{-1} cm^{-1} (610 nm)	3400 M^{-1} cm^{-1} (610 nm)
CT*	14260 ± 1300	4800 ± 680	4230 ± 250	{FLH– → NAD^+}[b] 2000 M^{-1} cm^{-1} (750 nm)	[2Fe–2S] (ox)[d] 570 M^{-1} cm^{-1} (750 nm)	2570 M^{-1} cm^{-1} (750 nm)
SQ	10890 ± 400	5900 ± 890	1300 ± 470	FNR(SQ)[c] 4400 M^{-1} cm^{-1} (610 nm)	[2Fe–2S] (red)[d] 570 M^{-1} cm^{-1} (610 nm)	4970 M^{-1} cm^{-1} (610 nm)
MC-3	7760 ± 730	5330 ± 100	970 ± 100			

[a] Data from Batie and Kamin (1986). [b] Data from Howell *et al.* (1972). [c] See Figure 1A. [d] See Figure 1B.

phase, shown by an increase in the absorbance at 740 nm (Figure 4A), as hydride transfer. This reaction forms a charge-transfer complex between $FMNH^-$ and NAD (CT*), contrasting with the previous postulate that this long wavelength absorbance was between oxidized FMN and NADH (Batie & Ballou, 1987). We now propose (Scheme 1) that the decay of CT* with a rate constant of 35 s^{-1} coincides with internal electron transfer from the reduced flavin to the iron–sulfur center to yield SQ, the species with flavin semiquinone and a reduced iron–sulfur center. This presumably also involves the release of NAD.

The Conundrum of Slow Electron Transfer. The PDR crystal structure shows that the interatomic distance between the 8-methyl group of the FMN and the sulfur of the closest ligand to the [2Fe–2S] center (Cys272) is only 4.7 Å. It is therefore surprising that intramolecular electron transfer over this distance is so slow (35 s^{-1}). In addition to distance, however, structural reorganization energy and differences in the relevant cofactor midpoint potentials in the complex can contribute to the electron transfer rate (Marcus & Sutin, 1985). Studies carried out with the closely related spinach ferredoxin-NADP reductase in complex with spinach ferredoxin demonstrate that electron transfer from the iron–sulfur center to the flavin occurs with a first-order rate constant >2000 s^{-1} (Walker *et al.*, 1991). The midpoint potentials have been measured for the FNR oxidized/FNR fully reduced couple (–360 mV), the FNR oxidized/semiquinone couple (–320 mV), and the FNR semiquinone/hydroquinone couple (–0.40 V) at pH 7.0 under conditions that permit semiquinone formation (Keirns *et al.*, 1972). A similar midpoint potential (–370 mV) was measured independently for the oxidized/hydroquinone couple for free FNR at pH 7.3. This potential was found to increase by about 20 mV upon complexation of FNR with ferredoxin (Smith *et al.*, 1981; Batie *et al.*, 1981). The midpoint potential of spinach ferredoxin is –420 mV and relatively pH independent (Tagawa *et al.*, 1967). However, this potential drops by more than 20 mV upon the formation of the ferredoxin–FNR complex (Smith *et al.*, 1981; Batie *et al.*, 1981). Thus, the difference between the FNR semiquinone/hydroquinone potential and the ferredoxin potential in the FNR–ferredoxin complex is at least 50 mV. This potential difference is clearly sufficient for eliciting rapid electron transfer. The flavin potential relevant for electron transfer in PDR is between that of CT* (the fully reduced flavin anion with [2Fe–2S] oxidized) and that of SQ (the neutral semiquinone with [2Fe–2S] reduced). Since CT* is a transient intermediate, we cannot measure the electrochemical potential difference between CT* and SQ. Our best estimate of the electrochemical driving force for the intramolecular electron transfer from the flavin to the [2Fe–2S] in PDR is 32 mV at pH 8. This comes from comparison of the fully reduced enzyme/SQ couple (E'_m = –269 mV) with the midpoint potential of the [2Fe–2S] center (E'_m = –237 mV at pH 8).

Although 32 mV of electrochemical potential difference (reduced flavin to [2Fe–2S]) would appear to be sufficient for electron transfer, it may be an overestimate since the redox states produced under equilibrium conditions in titrations can be different from those occurring in the kinetic electron-transfer step. In equilibrium titrations, the flavin semiquinone and the reduced iron–sulfur center are produced together since their redox potentials are virtually the same, and then the flavin becomes fully reduced. By contrast, the kinetic electron-transfer reaction is from enzyme with a reduced flavin anion to oxidized [2Fe–2S], resulting in an enzyme with a flavin semiquinone and a reduced [2Fe–2S]. Given the proximity of the two centers, it is conceivable that the potential of one cofactor would be affected by the redox state of the other, so that the potentials of the cofactors in the second step of the titration would be different from those in the kinetic reaction. Such an argument might explain an electrochemical driving force for electron transfer that is less than 32 mV.

The relatively slow electron transfer may be rationalized by a combination of factors. Electron transfer might involve significant structural reorganization; however, since the crystal structures of the oxidized and reduced forms are essentially the same (Correll *et al.*, 1992), current structural data do not support this idea. It should be noted that these structures do not represent the transition states or intermediates involved in the CT* to SQ electron-transfer process, so that it is conceivable that different conformations are involved, although such a finding would be quite unusual. Another possibility for the slow electron transfer in PDR is that the bound NAD, which is in charge-transfer interaction with the reduced flavin anion, as discussed above for CT*, increases the potential of the flavin to a value greater than the [2Fe–2S] potential (–237 mV). Although this would promote unidirectional hydride transfer to the flavin, it would also restrain electron transfer to the [2Fe–2S] center until NAD was released. Upon release of the NAD, the redox state of the flavin could return to –269 mV and electron transfer might be quite fast, as expected. Kinetically, this process would appear as a concerted release of NAD and electron transfer, as we have observed. In this manner the binding and release of NAD could partially regulate the electron transfer. It should be noted that during titrations with dithionite, no NAD is present. It would be of interest to measure electron-transfer rates in the absence and presence of NAD by independent methods, such as pulse radiolysis or flash photolysis. Interpretation of experiments with these techniques, it should be noted, will be difficult, since these experiments involve 1-electron transfers from external sources, and it will be difficult to poise the system

in the appropriate redox states for reproducing normal catalytic events.

There are other analogous systems with short interatomic distances between the iron–sulfur centers and the flavin that also exhibit anomalously slow electron transfer. The intermolecular electron transfer from the flavin of adrenodoxin reductase to adrenodoxin is only 5–6 s^{-1} (Lambeth & Kamin, 1979). It is known that the binding of pyridine nucleotide modulates the flavin potential in this system (Lambeth & Kamin, 1976). For example, NADP binds more tightly to reduced adrenodoxin reductase ($K_d = 1 \times 10^{-8}$ M) than to the oxidized enzyme ($K_d = 1.4 \times 10^{-5}$ M). The preferential binding of NADP to the reduced enzyme thus leads to an increase in the potential of the flavin by about 100 mV, which favors reduction of the flavin. Because NADP binding decreases the driving force for reduction of the adrenodoxin, it might be anticipated that the NADP is released before intermolecular electron transfer to the adrenodoxin occurs, which would be analogous to the intermolecular electron transfer in PDR as discussed earlier.

A similar enigma has been reported for trimethylamine dehydrogenase. Here, it has been shown by X-ray crystallography that the Cys353 ligand of the [4Fe–4S] center is only 4 Å from the 8-methyl position of the covalently bound FMN (Lim *et al.*, 1986). However, the rate of electron transfer from the flavin to the iron–sulfur center in the presence of substrate is only about 8 s^{-1} (Steenkamp *et al.*, 1978), whereas in the absence of substrate the rate is 250–1000 s^{-1}, depending on the pH (Rohlfs & Hille, 1991). EPR spectroscopy reveals an intense interaction between the flavin semiquinone and the iron–sulfur center, which occurs only in the presence of substrate (Stevenson *et al.*, 1986) or at high pH in the absence of substrate (R. J. Rohlfs and R. Hille, manuscript in preparation). This suggests that the relative positions or orientations of the two redox centers may change upon the binding of substrate. It would not be surprising if the orientation of the orbitals involved in electron transfer might also be important in determining the efficiency of electron transfer.

Binding of Pyridine Nucleotides to Reduced Forms of PDR. Our studies indicate that the absorbance of the 2-electron-reduced SQ intermediate is dependent on NADH concentration. Simulations required the incorporation of a step in which NADH binds to the SQ form of PDR, resulting in MC-3. The dissociation constant of this complex was estimated to be 10 μM from simulations of the data collected over a range of NADH concentrations. Simulation of the subsequent disproportionation reaction provided an independently determined value of this dissociation constant, 16 ± 5 μM, in substantial agreement with the value above. Both NAD and NADH binding processes are fast. However, NADH binds about 300-fold more tightly than NAD to the 2-electron-reduced PDR. Since, in the cell, it is likely that NADH is usually at a considerably higher concentration than NAD, complexes of the reduced enzyme with NADH (MC-3) are likely to be relevant in catalysis. Intermolecular electron transfer between the SQ form of PDR and a single-electron acceptor (in the case of disproportionation, a second molecule of the SQ form of PDR) is slow and therefore probably occurs between NADH complexes.

When a large excess of NAD is included in the reaction of oxidized PDR with stoichiometric NADH, two additional charge-transfer complexes (CT-2 and CT-3) are observed prior to the disproportionation phase of the reaction. However, the reduction kinetics up to the formation of SQ was not significantly affected by competitive binding of NAD under most of our experimental conditions. At very high (>10 mM NAD) concentrations, NAD competes with NADH for the pyridine nucleotide binding site on the oxidized enzyme and results in the formation of MC-2. This is evident in the retardation of the rates of steps preceding the formation of CT*. Since the binding constants for these complexes are quite weak (K_d = 3.7 mM), during normal catalysis these complexes will not be seen.

The results of this study complement and strengthen proposals based on the recently determined X-ray structure of PDR (Correll *et al.*, 1992), and they add one more member to the list of enzymes that show slow intramolecular electron transfer between closely spaced flavin and iron–sulfur cofactors.

ACKNOWLEDGMENT

We thank Drs. V. Massey and M. Ludwig from the Department of Biological Chemistry, University of Michigan, and Russell Hille from Ohio State University for many helpful discussions and critical evaluations of the manuscript. Samples of adrenodoxin were gifts from V. Massey. The FNR spectra were recorded in collaboration with Dr. G. Zanetti, Milan, Italy.

REFERENCES

Barshop, B. A., Wrenn, R. F., & Frieden, C. (1983) *Anal. Biochem. 130*, 134–145.

Batie, C. J., & Kamin, H. (1981) *J. Biol. Chem. 256*, 7756–7763.

Batie, C. J., & Kamin, H. (1986) *J. Biol. Chem. 261*, 11214–11223.

Batie, C. J., & Ballou, D. P. (1987) *Flavins & Flavoproteins* (Edmondson, D. E., & McCormick, D. B., Eds.) pp 377–380, Walter de Gruyter, Berlin.

Batie, C. J., & Ballou, D. P. (1990) *Methods Enzymol. 188*, 61–70.

Batie, C. J., LaHaie, E., & Ballou, D. P. (1987) *J. Biol. Chem. 262*, 1510–1518.

Batie, C. J., Ballou, D. P., & Correll, C. C. (1992) in *Chemistry & Biochemistry of Flavoenzymes* (Müller, F., Ed.) Vol. III, pp 543–556, CRC Press, Ann Arbor, MI.

Bevington, P. R. (1969) *Data Reduction & Error Analysis for the Physical Sciences*, pp 235–242, McGraw-Hill, Inc., New York.

Boyce, W. E., & Diprima, R. C. (1965) *Elementary Differential Equations & Boundary Value Problems*, pp 310–314, John Wiley & Sons, Inc., New York.

Bull, C., & Ballou, D. P. (1981) *J. Biol. Chem. 256*, 12673–12680.

Clark, M. W. (1960) *Oxidation Reduction Potentials of Organic Systems*, pp 487–500, The Williams & Wilkins Company, Baltimore, MD.

Correll, C. C., Batie, C. J., Ballou, D. P., & Ludwig, M. L. (1992) *Science 258*, 1604–1610.

Correll, C. C., Ludwig, M. L., Bruns, C. M., & Karplus, P. A. (1993) *Protein Sci. 2*, 2112–2133.

Cushman, D. W., Tsai, R. L., & Gunsalus, I. C. (1967) *Biochem. Biophys. Res. Commun. 26*, 577–583.

Howell, L. G., Spector, T., & Massey, V. (1972) *J. Biol. Chem. 247*, 4340–4350.

Hurley, J. K., Salomon, Z., Meyer, T. E., Fitch, J., Cusanovich, M. A., Markley, J., Cheng, H., Xia, B., Chae, Y. K., Medina, M., Gomez-Moreno, C., & Tollin, G. (1993) *Biochemistry 32*, 9346–9354.

Iyanagi, T., Makino, N., & Mason, H. S. (1974) *Biochemistry 13*, 1701–1710.

Kamin, H., Lambeth, J. D., & Siegel, L. M. (1980) in *Flavins & Flavoproteins* (Yagi, K., & Yamano, T., Eds.) pp 341–348, University Park Press, Baltimore.
Karplus, P. A., & Schulz, G. E. (1989) *J. Mol. Biol. 210*, 163–180.
Karplus, P. A., Daniels, M. J., & Herriott, J. R. (1991) *Science 251*, 60–66.
Keirns, J. J., & Wang, J. H. (1972) *J. Biol. Chem. 247*, 7374–7382.
Kimura, T., & Suzuki, K. (1967) *J. Biol. Chem. 242*, 485–491.
Kurzban, G. P., Howarth, J., Palmer, G., & Strobel, H. W. (1990) *J. Biol. Chem. 265*, 12272–12279.
Lambeth, D. J., & Kamin, H. (1976) *J. Biol. Chem. 251*, 4299–4306.
Lambeth, J. D., & Kamin, H. (1979) *J. Biol. Chem. 254*, 2766–2774.
Lim, L. W., Shamala, N., Mathews, F. S., Steenkamp, D. J., Hamlin, R., & Xuong, N. H. (1986) *J. Biol. Chem. 261*, 15140–15146.
Loesche, W., Wenz, I., Till, U., Petermann, H., & Horn, A. (1980) *Methods Enzymol. 66*, 11–23.
Lund, J., Woodland, M. P., & Dalton, H. (1985) *Eur. J. Biochem. 147*, 297–305.
Marcus, R., & Sutin, N. (1985) *Biochim. Biophys. Acta 811*, 265–322.
Mason, J. R., & Cammack, R. (1992) *Annu. Rev. Microbiol. 46*, 277–305.
Massey, V., & Palmer, G. (1962) *J. Biol. Chem. 237*, 2347–2358.
Massey, V., & Ghisla, S. (1974) *Ann. N.Y. Acad. Sci. 227*, 446–465.
Mayhew, S. G. (1970) *Biochim. Biophys. Acta 235*, 276–288.
Nishino, T., Nishino, T., Schopfer, L. M., & Massey, V. (1989) *J. Biol. Chem. 264*, 2518–2527.
Pai, E. F., Karplus, P. A., & Schultz, G. E. (1988) *Biochemistry 27*, 4465–4474.
Palmer, G., & Fee, J. A. (1971) *Biochim. Biophys. Acta 245*, 175–195.
Press, W. H., Teukolsky, S. A., Vetterling, W. T., & Flannery, B. P. (1992) *Numerical Recipes in C*, 2nd ed., pp 683–688, 707–752, Cambridge University Press, New York.
Rohlfs, R. J., & Hille, R. (1991) *J. Biol. Chem. 266*, 15244–15252.
Shieh, H., Ghisla, S., Hanson, L. K., Ludwig, M. L., & Nordman, C. E. (1981) *Biochemistry 20*, 4766–4774.
Shoun, H., Higashi, N., Beppu, T., Nakamura, S., Hiromi, K., & Arima, K. (1979) *J. Biol. Chem. 254*, 10944–10951.
Smith, M. J., Smith, W. H., & Knaff, D. B. (1981) *Biochim. Biophys. Acta 635*, 405–411.
Steenkamp, D. J., Singer, T. P., & Beinert, H. (1978) *Biochem. J. 169*, 361–369.
Stevenson, R. C., Dunham, W. R., Sands, R. H., Singer, T. P., & Beinert, H. (1986) *Biochim. Biophys. Acta 869*, 81–88.
Strickland, S., Palmer, G., & Massey, V. (1975) *J. Biol. Chem. 250*, 4048–4052.
Tagawa, K., & Arnon, D. I. (1967) *Biochim. Biophys. Acta 153*, 602–613.
Vieira, B. J., Colvert, K. K., & Davis, D. J. (1986) *Biochim. Biophys. Acta 851*, 109–122.
Walker, M. C., Pueyo, J. J., Navarro, J. A., Gomez-Moreno, C., & Tollin, G. (1991) *Arch. Biochem. Biophys. 287*, 351–358.
You, F. (1982) *Methods Enzymol. 87*, 101–126.
Zanetti, G., Morelli, D., Severino, R., Negri, A., Aliverti, A., & Curti, B. (1988) *Biochemistry 27*, 3753–3759.
Zimmerle, C. T., & Frieden, C. (1989) *Biochem. J. 258*, 381–387.
Zipples, M. F., & Staab, H. A. (1984) in *Flavins & Flavoproteins* (Bray, R. C., Engel, P. C., & Mayhew, S. G., Eds.) pp 21–24, Walter de Gruyter, Berlin.